Accurate Prediction of Alzheimer's Disease Using Multi-Modal MRI and High-Throughput Brain Phenotyping

Yun Wang[1], Chenxiao Xu[2], Seonjoo Lee[3], Yaakov Stern[4],
Jong Hun Kim[6], Shinjae Yoo[5], Hyoung Seop Kim[6], Jiook Cha[1]

1. Department of Psychiatry, Columbia University Medical Center , New York, NY, USA;
2. Department of Applied Mathematics, Stony Brook University, Stony Brook, NY, USA;
3. Department of Biostatistics, School of Public Health, Columbia University Medical Center, New York, NY, USA;
4. Department of Neurology, Columbia University Medical Center, New York, NY, USA;
5. Computatioal Science Initiative, Brookhaven National Laboratory, Upton, NY, USA;
6. Department of Neurology; Department of Rehabilitation Medicine, National Health Insurance Service Ilsan Hospital, Ilsan, Republic of Korea;

Corresponding to:

Jiook Cha, PhD
1051 Riverside Dr. New York, NY, 10032
Jiook.cha@nyspi.columbia.edu

Hyoung Seop Kim, MD
100 Ilsan-ro, Baekseok 1(il)-dong, Ilsandong-gu, Goyang-si, Gyeonggi-do, South Korea
rekhs@nhimc.or.kr

ABSTRACT

Accurate, reliable prediction of risk for Alzheimer's disease (AD) is essential for early, disease-modifying therapeutics. Multimodal MRI, such as structural and diffusion MRI, may contain multi-dimensional information neurodegenerative processes in AD. Here we tested the utility of structural MRI and diffusion MRI as imaging markers of AD using high-throughput brain phenotyping including morphometry and white-matter structural connectome (whole-brain tractography), and machine learning analytics for classification. We used a retrospective cohort collected at a dementia clinic (Ilsan Dementia Cohort; N=211; 110 AD, 64 mild cognitive impairment [MCI], and 37 subjective memory complaints [SMC]). Multi-modal MRI was collected (T1, T2-FLAIR, and diffusion MRI) and was used for morphometry, structural connectome, and white matter hyperintensity (WHM) segmentation. Our machine learning model trained on the large-scale brain phenotypes (n=34,646) classified AD, MCI, and SMC with unprecedented accuracy (AD/SMC: 97% accuracy, MCI/SMC: 83% accuracy; AD/MCI: 98% accuracy) with strict iterative nested ten-fold cross validation. Model comparison revealed that white-matter structural connectome was the primary contributor compared with conventional volumetric features (e.g., WHM or hippocampal volume). This study indicates promising utility of multimodal MRI, particularly structural connectome, combined with high-throughput brain phenotyping and machine learning analytics to extract salient features enabling accurate diagnostic prediction.

INTRODUCTION

There is an urgent, unmet need for clinically useful biomarkers of risk for Alzheimer's disease based on non-invasive and affordable measures suited for routine examination of individuals with subthreshold symptoms. Studies have focused on brain MRI-derived markers. Cortical thinning and reduced hippocampal volumes based on structural MRI are known for markers for Alzheimer's disease, but these structural estimates alone are insufficient for implementation at clinical settings because of insufficient accuracy and generalizability (*1*).

It is conceptualized that biomarkers of Aβ deposition first become abnormal early, and then ones of neuronal neurodegeneration or dysfunction show abnormality later in the disease (2). These markers of neurodegeneration, rather than those of Aβ or Tau proteinopathy appear more related to cognitive symptoms (2). While this model has been a guideline for biomarker development, yet there is an unmet need to add another crucial imaging marker—diffusion MRI and white matter.

Neurobiology of AD closely relates to axonal and neuronal degeneration followed by fibrillar lesions triggered by amyloid precursor protein (APP)-initiated death-receptor mechanism and activation of tau (*3, 4*). Initial axonal degeneration may lead to grey matter tissue changes and finally to neuronal loss or atrophy resulting in cognitive and functional impairment. Within this process, dMRI can be used to detect subtle changes in microstructure tissue properties in AD. DMRI uses water molecules an endogenous tracer to probe tissue microstructure or properties(*5*). Previous studies documented that decreased white matter integrity in associated with AD (*6-8*).

A potentially powerful application of dMRI to AD research is assessing axonal white matter tracts using tractography. Tractography is a computational reconstruction of white matter tracts using biophysical modeling of fiber orientations (*9, 10*). Thanks to recent advances in tractography algorithm, more accurate estimation of white matter tracts has been enabled (*11-14*) (cf., this technology has yet to reach the state-of-the-art status similarly to other MRI technologies (*15*)). In AD, human imaging of APP and tau shows widespread topography. Given this, when tractography is applied to the connectome level, this structural connectome data can be extremely useful for assessing axonal or white matter abnormalities across the entire connectome. A few studies using tractography at the connectome level started to reveal abnormal topological organization of structural connectome in Alzheimer's disease (*16, 17*). However, it remains untested whether to what extents the structural connectome carries additional information that structural MRI and morphometry analysis does not show. That is, what do we gain when including dMRI into the diagnostic model of AD?

In this study, we addressed this rigorously using optimized high-throughput MRI analysis, including morphometry and whole-brain diffusion tractography to estimate white-matter structure connectome, and machine learning and deep learning (graph convolutional neural network) algorithms for classification and prediction. To estimate more accurate, individualized structure connectome, we designed a rigorous dMRI preprocessing pipeline including several pre- and post-processing algorithms (e.g., denoising, bias field correction, and spherical-deconvolution

informed filtering of tractography [SIFT (*18*)] to exclude spurious streamlines). We performed this analysis in the structure (T1 and T2-FLAIR) and diffusion MRI collected from a retrospective clinical samples, Ilsan Dementia Cohort in South Korea (N=211; training data). Several machine learning models were trained on the large-scale brain phenotypes to make predictions of diagnosis (AD/MCI/normal or subjective memory complaints).

MATERIALS AND METHODS

Participants. We used data from 211 elderly people who visited the dementia clinic at National Health Insurance Service Ilsan Hospital, Goyang, South Korea from 2010 to 2015. This is a randomly selected subset of the Ilsan Dementia Cohort, a retrospective clinical cohort. Diagnosis was made by neurologists based on possible AD and Peterson's MCI criteria (*19*) clinical history taking, neuropsychological evaluations (seoul neuropyschological screening battery) and MMSE (Mini-Mental State Examination). Those with vascular dementia were included in the study. Those with AD as a primary diagnosis and with small vessel disease were noted as "AD with small vessel disease". Participants included 110 with diagnosis of Alzheimer's disease (AD; median age=82; interquartile intervals (Q3-Q1)=85-77), 64 with mild cognitive impairment (MCI; median age=73; Q3-Q1=77-66), and 37 subjective mild cognitive impairment (SMC; median age=74; Q3-Q1=78-72).

MRI acquisition. We had collected the following multimodal MRI from all participants: T1-weighted anatomical MRI, T2-weighted FLAIR, and diffusion MRI. T1: TE, 4.6 ms; matrix, 310 × 480× 480; voxel size, 0.5 × 0.5 × 0.5 mm. T2-FLAIR; matrix = 320 × 240 × 240; voxel size = 0.56 x 1.04 x 1.04. DMRI: matrix = 112 × 112 × 70; voxel size = 1.9 × 1.9 × 2.0 mm; the series included one image acquired without diffusion weighting and with diffusion weighting along 40 non-collinear directions (b = 600 s/m−2).

MRI Analysis-Structural MRI.

High-throughput computational analysis was conducted. Firstly, we estimated morphometrics measures using Freesurfer image analysis pipeline (*20*) (v6) from T1 and T2-FLAIR images. Morphometric measures (N=948 per subject) include volumes of the hippocampal subdivisions, and thickness, surface area, and volume of cortical/subcortical regions using two different atlases available in freesurfer (Desikan-Killiany atlas and Destrieux atlas; https://surfer.nmr.mgh.harvard.edu/fswiki/CorticalParcellation). The technical details of these procedures are described in previous studies (*21-24*). In brief, image processing includes motion correction, removal of non-brain tissue, Talairach transformation, segmentation, intensity normalization, tessellation of the gray matter white matter boundary, topology correction, and surface deformation. Deformation procedures use both intensity and continuity information to produce representations of cortical thickness. The maps produced are not restricted to the voxel resolution and are thus capable of detecting submillimeter differences between groups.

MRI Analysis-Diffusion MRI

We estimated structural connectome using the diffusion MRI analysis pipeline, Mrtrix 3 (*25*). The connectome measures (N= 33,698 per subject) include counts of streamlines, a surrogate measure of structural connectivity (*26-28*), and mean length of streamlines given any two brain regions based on multiple atlases. DWI was preprocessed using the following pipeline in Mrtrix. DWI was first denoised using a novel algorithm based on Random matrix theory that permits data-driven, non-arbitrary threshold for Principal Component Analysis denoising; this method enhances the DWI quality for quantitative and statistical interpretation (*29*). Denoised images then underwent eddy current and motion correction (*30*), brain extraction from three non-diffusion-weighted images (taking their median), and bias field correction using N4 algorithm

(N4ITK), an improved N3 method, in Advanced Normalization Tools (ANTs)(*31*). We then estimated fiber orientation distributions from each preprocessed data using 2nd-order integration over fiber orientation distributions (iFOD2). Based on the FODs, probabilistic tractography was performed using constrained spherical devolution (CSD). We used a target streamline count of 10 million across the whole brain. The tractograms were filtered using Spherical-Deconvolution Informed Filtering of Tractograms (SIFT) with a target streamline count of 3 million. After a primary statistical analysis using these filtered tractograms, we tested whether the effects of interest were robust to the tractography and filtering parameters, such as the target streamline count for tractography, SIFT, or a ratio between them. This method permits mapping streamline estimation back to individual's DWI, and updating a reconstruction to improve model fit. This approach renders the streamline counts connecting two brain regions proportional to the total cross-sectional area of the white matter fibers connecting those regions, enhancing streamline counts as a biologically plausible quantity, representing 'structural connectivity'. This was done by repeating tractography and SIFT with a set of extreme parameters (100 million and 5 million target streamlines, respectively) with a filtering factor of 20 (100/5). Finally, from the filtered tractograms, we generated a connectivity matrix in each participant using two different atlases available in freesurfer (Desikan-Killiany atlas (*23*) and Destrieux atlas (*24*)). We used streamline counts as the primary connectivity metric in this study as in a recent human infant imaging study (*32*), as well mean length as secondary measures. A prior macaque study suggests the validity of streamline counts as an indicator of fiber connection strength, with the number of streamlines significantly correlating with tract-tracing strength in the macaque brain (*33*). All the analysis codes will be available at online repository (https://github.com/jcha9928/adni_on_alcf)

Machine Learning Classification

We built several machine learning models using the large-scale brain MRI-derived phenotypes to predict diagnosis of AD and MCI, respectively. Two supervised classification models—logistic regression (L1 regularization) and linear support vector machine (SVM), were used. GridSearchCV from Scikit-Learn was utilized to search for the best combination of hyperparameter values (such as penalty parameter C and/or gamma) using cross validation for both models. For feature selection, we used 'Forests of randomized trees' method, an ensemble method to combine the predictions of base estimators built with a learning algorithm to improve generalizability and robustness (250 trees were used in this study). Repeated stratified 10-fold cross validation, iterated 10 times with different randomization in each was used. The feature selection procedure was done within cross validation.

We measured accuracy, sensitivity, specificity, F1 score, and receiver operating characteristic (ROC) curve from repeated 10-fold cross-validation to evaluate the performance of our classifiers. We built six different binary classifications, AD vs SMC, AD vs MCI, MCI vs SMC, AD only vs AD with small vessel issues, AD only vs MCI, AD only vs SMC. The preceding one before "vs" is always labeled as 1, and the latter one labeled as 0.   For example, in the AD vs SMC binary classification, we labelled AD population as positive 1, SMC as negative 0, then sensitivity can tell us the ratio of positive instances that are correctly detected by the classifier, and specificity can test the ability of this classifier to correctly identify those without AD. ROC and F1 score are also common and important tools used with classifiers. ROC curve plots the

true positive rate against the false positive rate. The area under the curve (AUC) was also used to compare two different classifiers. Each metric of performance has its own advantages and shortcomings for the evaluation of a classifier.

RESULTS

Classification of AD and MCI

Base model with age and sex only, without brain phenotypes classified the diagnosis of AD from MCI or SMC with around 70% ~ 80% accuracy. AD/SMC: 0.78 for LR and 0.77 for SVM; AD/MCI: 0.72 for LR and 0.71 for SVM. In contrast, Base model did not classify meaningfully MCI from SMC (0.58 for LR and 0.63 for SVM).

In classification of AD vs. SMC, "morphometry+connectome" model showed optimal classification accuracy (SVM accuracy = 0.97 ± 0.039; LR accuracy=0.96 ± 0.05; ten iterations of nested ten-fold cross validation) (**Table 2; Figure 1 & 2**). While "connectome" model showed similar accuracy (SVM accuracy = 0.98 ± 0.032; LR accuracy=0.98 ± 0.043), "morphometry" model showed least significant accuracy (SVM accuracy = 0.85 ± 0.10; LR accuracy=0.86 ± 0.102).

In classification of MCI vs. SMC, "morphometry+connectome" models also showed good classification accuracy (SVM accuracy=0.83 ± 0.11; LR accuracy=0.82 ± 0.15) (**Table 2; Figure 1 & 2**). While "connectome" model showed similar accuracy (SVM accuracy = 0.77 ± 0.14; LR accuracy=0.79 ± 0.165), "morphometry" model showed poor performance (SVM accuracy = 0.51 ± 0.146; LR accuracy=0.51 ± 0.179).

In classification of AD vs. MCI, "morphometry+connectome" models showed good classification accuracy (SVM accuracy=0.98 ± 0.03; LR accuracy=0.97 ± 0.039) (**Table 2; Figure 1 & 2**). While "connectome" model showed similar accuracy (SVM accuracy = 0.98 ± 0.03; LR accuracy=0.97 ± 0.048), "morphometry" model showed least significant accuracy (SVM accuracy = 0.78 ± 0.094; LR accuracy=0.80 ± 0.118).

DISCUSSION

In this study, we showed that large-scale MRI-derived brain phenotypes, morphometry and structural connectome, could be used to accurately classify Alzheimer's Disease (AD) and Mild Cognitive Impairment (MCI). The final model reported here, based on 211 elders, showed optimal classification in AD and MCI. Given that the quality of the MRI was standard (e.g., T1 MPRAGE, T2-FLAIR, and diffusion MRI with 28 gradient directions and b value of 800 s/m−2 from a 3 Telsa magnet), our results show the potential utility of multi-modal MRI combined with high-throughput brain phenotyping for screening in clinical settings.

The classification accuracy of our combined models exceeds the state-of-the-art results reported in the literature. A recent review study (*34*) shows the current state-of-the-art classification accuracy using multimodal biomarkers (including invasive ones) is 95% (AD/normal), 82% (MCI/normal: structural MRI, fluorodeoxyglucose-PET, and CSF Aβ42, CSF t-tau, and CSF p-tau (*35*), and 82.7% (*36*) (AD/MCI: structural MRI and PET). Compared with these studies, our results present more accurate diagnostic performance. Though remaining to be tested in independent samples, this strongly indicates the feasibility of multi-modal MRI, particularly diffusion MRI-based structural connectome, as an accurate brain marker of the disease.

Our samples represent a retrospective clinical cohort. Compared to some of the publicly available imaging databases for AD research, our clinical data may present a greater heterogeneity in aging samples; therefore, these samples may well represent a true clinical population. Given this, it is interesting such an accurate classification for both AD and MCI. However, in classifying AD/SMC, given the significant difference in age (i.e., greater in the AD group), it is likely that a greater aging effect embedded on morphometric and connectomic estimates contributed to the perfect classification. Owing to the lack of age-matched healthy controls, in this study we could not disentangle impact of normal and pathological (i.e., AD) aging on brain phenotypes. This remains to be tested in future research.

On the other hand, the accurate classification of MCI/SMC (age-matched) is notable. Our analysis showed the most significant contributor to this model was structural connectome. The connectome model classified MCI/SMC as equally accurate as the combined model, whereas the morphometry model did not classify accurately. This pattern was particularly more pronounced in MCI/SMC classification than in AD/SMC classification. This may reflect different time ordering of white matter integrity (or connectivity) and grey matter atrophy. Literature shows capability of dMRI-derived measures to detect subtle changes in tissue properties or microstructure, whereas structural MRI is typically used to estimate macroscopic properties, namely volume.

Diffusion MRI uses signals related to Brownian diffusion of water molecules, and is hence sensitive to subtle changes in tissue properties. In brain tissue, directions of water diffusion are governed by the geometry of the tissue (*6*). Thus, diffusion MRI uses water molecules an endogenous tracer to probe tissue microstructure or properties(*37*). While histopathological validation of dMRI signals is an active area of research in cancer biology (*38*), in brain imaging,

9

such validation remains limited. In AD research, dMRI metrics, such as diffusivity or anisotropy, typically estimated using tensor model, show associations between abnormal microstructural properties of the white matter and preclinical AD (*37*). In a broader context of brain insults, such as obstructive sleep apnea, we have shown that dMRI-based microstructural index, mean diffusivity within the hippocampus, is more sensitive to cognitive changes compared with hippocampal atrophy estimated from structure MRI (*39*). Another study confirmed the superior sensitivity of the dMRI-based "microscopic" metrics relative to sMRI-based "macroscopic (volumetric)" measures in accounting for cognitive and functional abnormalities in individuals with depression (*40*). These support the potential utility of dMRI as an early indication of abnormal tissue properties (due to neuronal injury or degeneration) in AD. It is possible that the greater contribution of structure connectome abnormalities than brain atrophy in classifying MCI may reflect subtle changes in white matter structural connectome in MCI before severe degeneration, that is, brain atrophy.

Given the unexpectedly accurate classification of MCI/SMC, we predict that structural connectome may contain salient information additional to morphometry, essential to predict a subtler clinical outcome than current diagnosis, such as prognosis or mortality. Future study should examine this in retrospective clinical data, ideally using rigorous imaging analytics with optimal brain phenotyping technology that permit accurate estimation of phenotypes. Positive results from such a retrospective study will then lead to prospective clinical studies to test clinical utility of connectome-based MRI markers. In sum, this study lends a strong support for white matter structural connectome estimated using diffusion tractography as a method towards an accurate, clinically useful imaging marker of AD.

Acknowledgements

Tables

Table 1. Participant Demographics

	AD	MCI	SMC	Test Statistics	P value
Age, Mean (SD)	79.95(6.61)	71.42 (8.62)	72.25 (6.99)	F = 32.72	P < 0.001
Sex					
Female	74	38	32	χ^2 =8.56	P = 0.014
Male	36	24	4		

Table 2. Combined Machine Learning Classifier Performances

	AD vs MCI	AD vs SMC	MCI vs SMC	ADonly vs AD with small vessels	ADonly vs MCI	ADonly vs SMC
LR Accuracy (Mean±SD)	.98±.05	.96±.05	.82±.15	.93±.09	.95±.08	.94±.07
LR sensitivity(Mean±SD)	.99±.03	.98±.03	.86±.10	.92±.07	.92±.06	.93±.05
LR specificity(Mean±SD)	.98±.05	.96±.05	.82±.15	.93±.09	.95±.08	.94±.07
LR F1s (Mean±SD)	.99±.05	1.0±.00	.86±.10	.84±.01	.92±.06	.90±.05
SVM Accuracy (Mean±SD)	.98±.03	.97±.04	.83±.11	.89±.09	0.91±.07	0.90±.06
SVM sensitivity (Mean±SD)	1.0±.00	1.0±.00	.85±.19	.78±.22	0.85±.14	0.83±.13
SVM specificity (Mean±SD)	.98±.03	.98±.03	.84±.10	.80±.11	0.91±.07	0.88±.07
SVM F1s (Mean±SD)	1.0±.00	1.0±.00	.85±.19	.78±.22	0.85±.14	0.83±.13

**LR, logistic regress; SD, standard deviation; SVM, support vector machine.**

Figures

Figure 1. Diagnostic measures of morphometric, connectome, and combined model.
Measures of diagnostic performances used are diagnostic accuracy, sensitivity, specificity, and F1. Measures were averaged across iterative cross-validation splits. In most of the measures, combined model (i.e., morphometry and connectome estimates) showed the maximal performances.
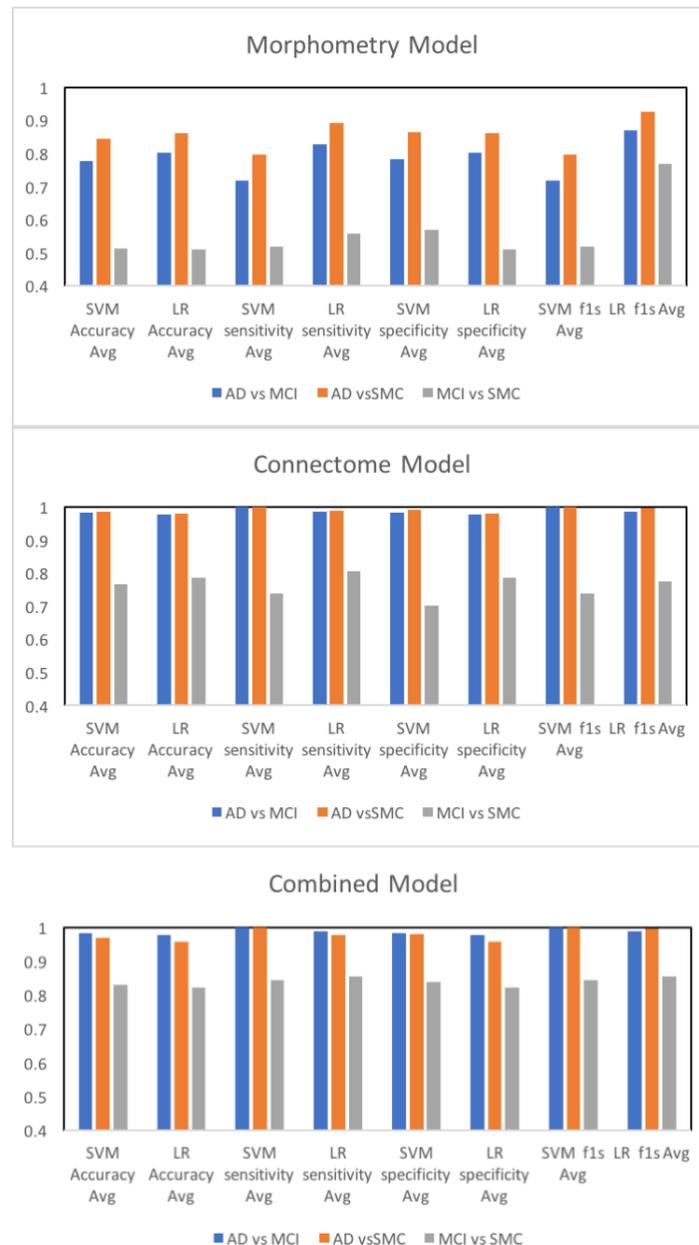
Figure 2. Receiver-Operator Characteristic (ROC curve) Analysis. Combined models ("morphometry+connectome") accurately classified AD, MCI, and SMC. (a) AD vs SMC classification; (b) MCI vs SMC classification; (C) AD vs MCI classification. Logistic Regression and SVM classifiers have similar area-under-curve (AUC) for different binary classifications.

Receiver-Operator Characteristic Plot
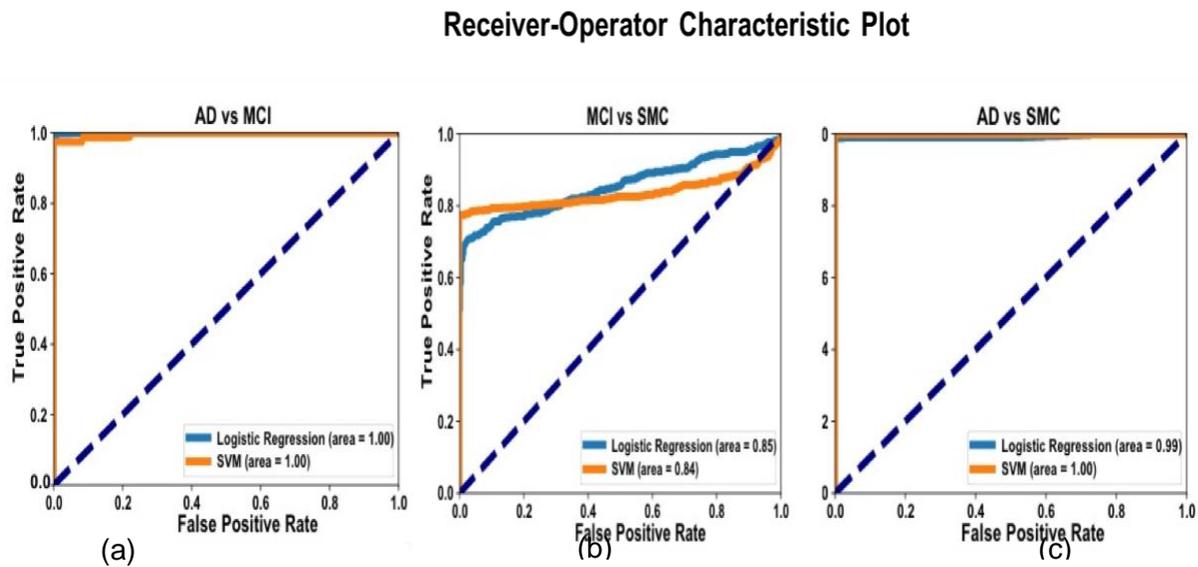
References

1. S. Teipel *et al.*, Multimodal imaging in Alzheimer's disease: validity and usefulness for early detection. *Lancet Neurol* **14**, 1037-1053 (2015).

2. C. R. Jack, Jr. *et al.*, Hypothetical model of dynamic biomarkers of the Alzheimer's pathological cascade. *Lancet Neurol* **9**, 119-128 (2010).

3. A. Nikolaev, T. McLaughlin, D. D. O'Leary, M. Tessier-Lavigne, APP binds DR6 to trigger axon pruning and neuron death via distinct caspases. *Nature* **457**, 981-989 (2009).

4. D. M. Holtzman, J. C. Morris, A. M. Goate, Alzheimer's disease: the challenge of the second century. *Sci Transl Med* **3**, 77sr71 (2011).

5. C. Beaulieu, The basis of anisotropic water diffusion in the nervous system - a technical review. *NMR Biomed* **15**, 435-455 (2002).

6. G. Douaud *et al.*, DTI measures in crossing-fibre areas: increased diffusion anisotropy reveals early white matter alteration in MCI and mild Alzheimer's disease. *Neuroimage* **55**, 880-890 (2011).

7. Y. Zhang *et al.*, White matter damage in frontotemporal dementia and Alzheimer's disease measured by diffusion MRI. *Brain* **132**, 2579-2592 (2009).

8. J. Acosta-Cabronero, G. B. Williams, G. Pengas, P. J. Nestor, Absolute diffusivities define the landscape of white matter degeneration in Alzheimer's disease. *Brain* **133**, 529-539 (2010).

9. A. K. Seehaus *et al.*, Histological validation of DW-MRI tractography in human postmortem tissue. *Cereb Cortex* **23**, 442-450 (2013).

10. H. Johansen-Berg, T. E. Behrens, Just pretty pictures? What diffusion tractography can add in clinical neuroscience. *Curr Opin Neurol* **19**, 379-385 (2006).

11. O. Sporns, The human connectome: a complex network. *Ann N Y Acad Sci* **1224**, 109-125 (2011).

12. Y. Shi, A. W. Toga, Connectome imaging for mapping human brain pathways. *Mol Psychiatry* **22**, 1230-1240 (2017).

13. H. Azadbakht *et al.*, Validation of High-Resolution Tractography Against In Vivo Tracing in the Macaque Visual Cortex. *Cereb Cortex* **25**, 4299-4309 (2015).

14. O. Ciccarelli, M. Catani, H. Johansen-Berg, C. Clark, A. Thompson, Diffusion-based tractography in neurological disorders: concepts, applications, and future developments. *Lancet Neurol* **7**, 715-727 (2008).

15. K. H. Maier-Hein *et al.*, The challenge of mapping the human connectome based on diffusion tractography. *Nat Commun* **8**, 1349 (2017).

16. C. Y. Lo *et al.*, Diffusion tensor tractography reveals abnormal topological organization in structural cortical networks in Alzheimer's disease. *J Neurosci* **30**, 16876-16885 (2010).

17. Z. Dai, Y. He, Disrupted structural and functional brain connectomes in mild cognitive impairment and Alzheimer's disease. *Neurosci Bull* **30**, 217-232 (2014).

18. R. E. Smith, J. D. Tournier, F. Calamante, A. Connelly, The effects of SIFT on the reproducibility and biological accuracy of the structural connectome. *Neuroimage* **104**, 253-265 (2015).

19. R. C. Petersen, Mild cognitive impairment as a diagnostic entity. *Journal of internal medicine* **256**, 183-194 (2004).

20. B. Fischl, FreeSurfer. *Neuroimage* **62**, 774-781 (2012).

21. B. Fischl, M. I. Sereno, A. M. Dale, Cortical surface-based analysis. II: Inflation, flattening, and a surface-based coordinate system. *Neuroimage* **9**, 195-207 (1999).

22. B. Fischl, A. M. Dale, Measuring the thickness of the human cerebral cortex from magnetic resonance images. *Proc Natl Acad Sci U S A* **97**, 11050-11055 (2000).

23. R. S. Desikan *et al.*, An automated labeling system for subdividing the human cerebral cortex on MRI scans into gyral based regions of interest. *Neuroimage* **31**, 968-980 (2006).

24. C. Destrieux, B. Fischl, A. Dale, E. Halgren, Automatic parcellation of human cortical gyri and sulci using standard anatomical nomenclature. *Neuroimage* **53**, 1-15 (2010).

25. J. D. Tournier, F. Calamante, D. G. Gadian, A. Connelly, Direct estimation of the fiber orientation density function from diffusion-weighted MRI data using spherical deconvolution. *Neuroimage* **23**, 1176-1185 (2004).

26. J. Cha *et al.*, Effects of Serotonin Transporter Gene Variation on Impulsivity Mediated by Default Mode Network: A Family Study of Depression. *Cereb Cortex*, 1-11 (2017).

27. J. Cha *et al.*, Abnormal reward circuitry in anorexia nervosa: A longitudinal, multimodal MRI study. *Hum Brain Mapp* **37**, 3835-3846 (2016).

28. J. Cha *et al.*, Neural Correlates of Aggression in Medication-Naive Children with ADHD: Multivariate Analysis of Morphometry and Tractography. *Neuropsychopharmacology* **40**, 1717-1725 (2015).

29. J. Veraart *et al.*, Denoising of diffusion MRI using random matrix theory. *Neuroimage* **142**, 394-406 (2016).

30. J. L. Andersson, S. N. Sotiropoulos, An integrated approach to correction for off-resonance effects and subject movement in diffusion MR imaging. *Neuroimage* **125**, 1063-1078 (2016).

31. N. J. Tustison *et al.*, N4ITK: improved N3 bias correction. *IEEE Trans Med Imaging* **29**, 1310-1320 (2010).

32. M. P. van den Heuvel *et al.*, The Neonatal Connectome During Preterm Brain Development. *Cereb Cortex* **25**, 3000-3013 (2015).

33. M. P. van den Heuvel *et al.*, Comparison of diffusion tractography and tract-tracing measures of connectivity strength in rhesus macaque connectome. *Hum Brain Mapp* **36**, 3064-3075 (2015).

34. S. Rathore, M. Habes, M. A. Iftikhar, A. Shacklett, C. Davatzikos, A review on neuroimaging-based classification studies and associated feature extraction methods for Alzheimer's disease and its prodromal stages. *Neuroimage* **155**, 530-548 (2017).

35. X. Zhu, H. I. Suk, D. Shen, A novel matrix-similarity based loss function for joint regression and classification in AD diagnosis. *Neuroimage* **100**, 91-105 (2014).

36. Y. D. Zhang, S. H. Wang, Z. C. Dong, Classification of Alzheimer Disease Based on Structural Magnetic Resonance Imaging by Kernel Support Vector Machine Decision Tree. *Prog Electromagn Res* **144**, 171-184 (2014).

37. A. R. Hoy *et al.*, Microstructural white matter alterations in preclinical Alzheimer's disease detected using free water elimination diffusion tensor imaging. *PLoS One* **12**, e0173982 (2017).

38. D. M. Patterson, A. R. Padhani, D. J. Collins, Technology insight: water diffusion MRI--a potential new biomarker of response to cancer therapy. *Nat Clin Pract Oncol* **5**, 220-233 (2008).

39. J. Cha *et al.*, The Effects of Obstructive Sleep Apnea Syndrome on the Dentate Gyrus and Learning and Memory in Children. *J Neurosci* **37**, 4280-4288 (2017).

40. J. Cha *et al.*, Abnormal hippocampal structure and function in clinical anxiety and comorbid depression. *Hippocampus* **26**, 545-553 (2016).